Variation in resonant Auger yields into the $^1G_4$·nl states of Kr across the L_3 threshold

K Okada[1], M Kosugi[1], A Fujii[2], S Nagaoka[2], T Ibuki[3], S Samori[3], Y Tamenori[4], H Ohashi[4], I H Suzuki[5] and K Ohno[1]

[1]Department of Chemistry, Hiroshima University, Higashi-Hiroshima 739-8526, Japan

[2]Department of Fundamental Material Science, Ehime University, Matsuyama 790-8577, Japan

[3]Kyoto University of Education, Kyoto 612-8522, Japan

[4]Japan Synchrotron Radiation Research Institute/SPring-8, Hyogo 679-5198, Japan

[5]National Metrology Institute of Japan/AIST, Tsukuba 305-8568, Japan

E-mail: okadak@sci.hiroshima-u.ac.jp

Abstract

Resonant Auger transitions into $^1G_4$·nl states following Kr $2p_{3/2}$ electron excitation have been measured using monochromatized undulator radiation and a hemispherical electron energy analyzer. A clear identification of electron peaks was made for the $^1G_4$·5s, $^1G_4$·4d, $^1G_4$·5d and so forth when the photon energy approached to the ionization threshold. The formation of the $^1G_4$·4d state was found over a relatively wide energy range across the threshold, because of the short lifetime of the 2p hole and of shake effects in electron emission processes. The angular dependence of these decays showed little effect on the polarization direction of the incident photon, which suggests that little anisotropy is related to that of the normal Auger transition into the $^1G_4$ state.

1. Introduction

Excitation or ionization of an inner-shell electron produces a vacancy state, which rapidly relaxes by a radiative or radiationless process [1–6]. The process has long been studied from standpoints of fundamental interest and application for determining electronic structures of some materials. Recent advancement of synchrotron radiation technique has enabled us to record X-ray absorption near-edge structures (XANES) with ease, and these spectra generally focus on the inner-shell excited states. Vacancy-decay spectra, on the other hand, are very sensitive to dynamical processes in the highly excited states, as shown by theoretical formalisms which regard X-ray absorption and vacancy decay as a one-step resonant Raman scattering [1–4]. This scattering is largely affected by a short lifetime of an intermediate excited state and supposed to play a crucial role on shake effects and photoelectron recapture, being related to core relaxation and interference among intermediate amplitudes.

Resonant Auger transitions connected with shallow cores of rare gas atoms have been studied by several research groups [1,3,5–9]. In many cases the excited electron behaves as a spectator, but occasionally the electron is excited into higher orbitals with the same azimuthal quantum number, called shake-up transition. These final states are also produced by the photoelectron recapture (one of post-collision interaction effects, PCI effects) near the ionization threshold [10–13]. Such phenomena have been identified in the decay from Ar $1s^{-1}np$ and Xe $2p^{-1}nd$ states [2,4]. Similar effects are presumed to occur in the instance of Kr $2p^{-1}nl$ states at about 1.7 keV above the ground state, but it had been difficult to pursue to excite these electrons using monochromatic soft X-rays owing to no available light source with sufficient intensity in this energy region. However, the effort by Japanese scientists has realized the utilization of a brilliant undulator radiation combined with a grating monochromator employing ultra-grazing incidence optical elements covering photon energies above 1.5 keV [14–16].

Photoabsorption spectrum of Kr 2p electrons was observed by some researchers and the excited states with higher principal quantum numbers were reported [17–19]. Normal Auger electron spectra using charged-particle techniques were observed and analyzed, which showed that the $^1G_4$ final state yields the strongest peak in the electron kinetic-energy region near 1460 eV [20–22]. The resonant Auger transitions were found from the $2p^{-1}nl$ states by the present authors, who used monochromatized undulator radiation combined with the grating monochromator having high resolving power [23,24]. The final states of $^1G_4{\cdot}5s$ and $^1G_4{\cdot}4d$ were identified at several photon energies around the $2p_{3/2}$ threshold.

In the present study, electron emission spectra of Kr have been measured in the photon energy region of 1670 eV through 1695 eV using a high-resolution electron spectrometer, SES-2002. The final states with the principal quantum numbers of 5 through 7 were discovered through a peak-fitting analysis. The electron spectra observed in the direction perpendicular to the photon polarization

efficiently served to obtain a better fitting because of no severe overlapping of the photoelectron peaks from the outer $3p_{1/2}$ and $3p_{3/2}$ orbitals.

2. Experimental

The experiments were performed on the c branch of the soft X-ray photochemistry beamline BL27SU at the SPring-8 facility [14–16]. The beamline provides linearly polarized monochromatic light ranging from 0.2 keV to 2.5 keV, and the degree of polarization is higher than 0.98 at the tuning of the first-order radiation with the horizontal polarization [25]. At the tuning of the 0.5th-order radiation, we can utilize the linear polarization in the vertical direction [15]. The energy calibration of the monochromator was performed using the Kr $2p_{3/2}\rightarrow5s$ and Ne $1s\rightarrow3p$ transitions [17,18,24,26]. The intensity of the monochromatized incident photon beam during the measurement was monitored by collecting the drain current of the post-focusing mirror on the beamline. Sample gas of Kr (stated purity >99.995%) was purchased from Taiyo Toyo Sanso Co., Ltd. and supplied into the main chamber under about 1×10^{-3} Pa during the measurements of ion yield curves. The ion yields were measured using a time-of-flight mass analyzer attached to the main chamber [16,23,24]. An electric field of 50 V/mm was applied across the ionization region and produced Kr ions were detected with a microsphere plate (MSP; El-Mul Technologies, C0180DTA). These ions were observed in the mode of total ion yield measurement with a photon bandwidth of 0.4 eV.

An electron spectrometer is positioned 3.2 m downstream from the mass analyzer and the spectrometer consists of a hemispherical electron energy analyzer (Gammadata Scienta, SES-2002) fitted to a gas cell (GC-50) by way of a multi-element lens in a differentially pumped chamber [24,25,27]. The gas density observed was 6×10^{-3} Pa just outside the gas cell during the measurements. The emitted electrons were measured at the horizontal direction and the angular distributions of electrons were obtained by tuning the gap distance of the Figure-8 undulator for selecting the first- or 0.5th-order light. The pass energy of the spectrometer was fixed at 500 eV for maximizing electron signals owing to low signal rates for high-energy electrons. The spectrometer parameters were set such that the resolution of the electron spectra was about 0.73 eV for Auger electrons and 3p photoelectrons. The photon bandwidth employed was 0.45 eV. The photon flux monitor was calibrated against the discrimination effect on the polarization using the observed normal Auger spectra from the L_2 hole state that are isotropic [22]. The electron energy was calibrated using the peak energy for the $^1G_4$ state produced through the Auger decay from the L_3 hole state [21]. The photon energy was confirmed to be correct by measuring the 3p photoelectrons (ionization thresholds: 214.4 and 222.2 eV [28]) and the resonant Auger electron of the $^1G_4$·4d state.

3. Results and discussion

3.1. Ion yield spectrum

The total ion yield spectrum of Kr is shown in the photon energy region of 1670–1685 eV in figure 1. The bar with hatching denotes the ionization threshold of the $2p_{3/2}$ electron at 1678.4 eV [28]. It is found that the spectrum shows a small maximum at 1673.8 eV, a shoulder at 1676.1 eV and the highest yield at about 1679 eV. The first structure (1673.8 eV) is assigned to the transition to the $2p_{3/2}^{-1}5s$ state, which is in agreement with previous studies [17,18,23]. The second structure stems from the excitation into the 4*d* orbital, as seen in the previous data [24]. Many years ago, a series of resonance lines was observed by means of a photographic plate technique [17], but the present spectrum does not exhibit clear structures above 1676.5 eV. The present findings for unresolved structure of high Rydberg excitation are supposed to originate from broadening due to the short lifetime of the $2p_{3/2}$ hole.

3.2. Electron kinetic energy spectrum

Figure 2 shows electron kinetic energy spectra of Kr at several photon energies across the $2p_{3/2}$ ionization threshold. The spectra measured in the direction parallel to the photon polarization are illustrated on a lifted baseline and those in the perpendicular direction are plotted on a normal baseline. The photon energy where the spectrum was measured is added at the right end of each panel in figure 2.

The spectrum in the parallel direction at the lowest photon energy shows only the photoelectron peaks from the outer $3p_{1/2}$ and $3p_{3/2}$ orbitals. The intensity ratio for these peaks is close to 1:2, the ratio of multiplicity. That of the perpendicular direction shows unclear structures with low intensities. This finding comes from the fact that these photoelectrons have positive anisotropy parameters far away from the ionization thresholds. The theoretical work predicts that the parameters are about 1.5 in this photon energy region [29,30]. The present estimation proposes that those are about 1.7 although experimental uncertainties are relatively large.

When the photon energy comes up slightly above the excitation energy into the $2p_{3/2}^{-1}5s$ state (1674.2 eV), small structures around 1466 eV show up in the spectra in the both directions. These structures are mainly ascribed to the transitions into the final states of $^1G_4{\cdot}5s$ and $^1G_4{\cdot}4d$ resonant Auger transitions [24]. The transition strengths in the two directions for each of these final states are close to each other. At the photon energy of 1676.6 eV, the photoelectron peak of the $3p_{3/2}$ orbital is positioned around 1462 eV and the resonant Auger electron peak of the $^1G_4{\cdot}4d$ exists near 1468 eV. Small structures around 1473 eV originate from the transitions into the $^3F_J{\cdot}4d$ (J = 2, 3, 4) states [24].

The peak at 1462.5 eV in the perpendicular spectrum probably stems from the transitions into a $^1G_4$·nd state, where n is 5 or 6. The corresponding peak in the parallel direction overlaps with the $3p_{3/2}$ photoelectron peak.

When the photon energy increases further, both spectra in the two directions become complicated due to the emergence of the resonant Auger decays into higher Rydberg orbitals and of the normal Auger decays (diagram lines) and due to the overlapping of these decays with the $3p_{3/2}$ photoelectron peak. Above the ionization threshold the diagram decays indicate higher intensities with some tailing into a higher energy side and the $3p_{1/2}$ photoelectron peak overlaps with the diagram peaks, in particular at the photon energy of 1680.4 eV in figure 2.

3.3. Peak-fitting procedure

In order to disentangle the complex peak structures shown in figure 2, we have employed a peak-fitting technique. Voigt functions were used for the photoelectrons and resonant Auger electrons. The width of the experimental instruments was estimated to be 0.85 eV. The lifetime widths reported so far vary for the $3p_{1/2}$ and $3p_{3/2}$ photoelectrons [17,31,32] and in the present study they were evaluated by a peak-fitting analysis for the spectrum acquired at the photon energy of 1670.9 eV. The widths of 1.39 and 1.29 eV were obtained for the $3p_{1/2}$ and $3p_{3/2}$ photoelectrons, respectively. The lifetime width of 0.16 eV was assumed for the resonant Auger electrons of the $3d^{-2}$nl configurations. In addition, in the energy range of interest the normal Auger peaks are distorted through the post-collision interaction (PCI), and these peaks can be approximated with the following equation [10,22,33–36]:

$$y = \frac{H}{1+\varepsilon^2} \times \frac{\pi\xi}{\sinh(\pi\xi)} \exp(2\xi \arctan\varepsilon) . \quad (1)$$

In this equation, H denotes relative peak intensity and ξ indicates a parameter expressing the magnitude of distortion, which was used here as an adjustable parameter. The term ε is represented using the lifetime of the $2p_{3/2}$ hole, Γ, and the energy difference as follows:

$$\varepsilon = \frac{2(E_0 - E)}{\Gamma} \quad (2)$$

where E_0 and E are the peak energy and electron kinetic energy, respectively. The value of 1.11 eV was used here for Γ. Throughout the fitting procedure the relative intensities for individual Auger multiplets were kept such that those accord with the intensity ratios of the normal Auger peaks ($^1S_0$, $^1G_4$, $^3P_{0,1}$, $^3P_2$, $^1D_2$, $^3F_2$, $^3F_3$ and $^3F_4$) measured at the photon energy of 1725 eV [27]. Some examples of the fitting results are shown in figures 3 and 4. Figure 3 exhibits the results fitted for the spectra observed in the parallel direction at 1674.2, 1676.6, 1677.5, 1680.4 and 1695.5 eV. The fitted spectra

for those in the perpendicular direction at the same photon energies are displayed in figure 4. The thin curves denote the calculated components for the photoelectrons, resonant Auger electrons and diagram Auger lines, and the thick curves indicate the summation of them. The calculated curves at all the photon energies have well reproduced the measured electron kinetic energy spectra. For the normal Auger peaks, values of the asymmetry parameter ξ obtained by the fitting procedure change reasonably: from 1.72 for the photon energy of 1678.6 eV to 0.53 in the case of the 1695.5-eV photons. This finding suggests that the functions used here and the estimation of peak positions are reasonable.

At the photon energy of 1676.6 eV, the peak at 1467.6 eV is assigned to the $^1G_4{\cdot}4d$ and the structures at the higher energies are mainly ascribed to the $^3F_J{\cdot}4d$ (J = 2, 3, 4) final states. The peak at 1462.6 eV in the perpendicular spectrum (figure 4) comes from the resonant Auger decay into $^1G_4{\cdot}5d$, and that at 1460.8 eV corresponds to the decay to the $^1G_4{\cdot}6d$ final state. Therefore the spectrum in the parallel direction (figure 3) has been decomposed into the $^1G_4{\cdot}5d$, $^1G_4{\cdot}6d$ and $3p_{3/2}$ photoelectron peaks in the region of 1460–1464 eV. A hump around 1465.3 eV is supposed to consist of the $^1G_4{\cdot}6s$ state mainly. Another possibility is a transition into the $^1D_2{\cdot}5d$ or $^3F_3{\cdot}6d$ state, although the transition strength into the latter state is presumed to be low at this photon energy. A small peak at 1455 eV originates from the decay into the $^1S_0{\cdot}5d$ state. Similar situations were found in the spectra at the photon energy of 1677.5 eV, indicating that the structure around 1463 eV is composed of the peaks by the transitions to the $^1G_4{\cdot}nd$ (n = 5, 6, 7) states and the $3p_{3/2}$ photoelectron. At the photoabsorption step, main excitation is considered to occur into the $2p_{3/2}^{-1}5d$ state based on the ionization energy of 1678.4 eV. The considerable yields of the higher quantum number states probably originate from the shake-up process in the electron emission.

At the photon energy of 1680.4 eV, the structures around 1461 eV between the $3p_{1/2}$ and $3p_{3/2}$ photoelectron peaks are ascribed to the diagram transitions, which have asymmetric peak shapes induced through the PCI with the $2p_{3/2}$ photoelectron. This photon energy is positioned well above the ionization threshold. However, the resonant Auger peaks of the $^1G_4{\cdot}4d$ and its relatives are still seen around 1471.5 eV. This finding is presumed to be connected with the short lifetime of the 2p hole and possibly to be yielded through the recapture of slow photoelectrons by the PCI. When the photon energy reaches 1695.5 eV, considerably above the threshold, the peaks for resonant Auger transitions disappear and the observed peaks come from the diagram lines with some PCI distortion and the $3p_{1/2}$ and $3p_{3/2}$ photoelectrons.

3.4. Assignment of the resonant Auger peaks

Based on the peak-fitting results, we have assigned the peaks identified in the spectra of the electron kinetic energy as those given in Table 1. Only the states connected with the $^1G_4$ term are listed.

The photon energy is denoted at the left end and the quantum number of the spectator electron is listed at the top row. The term values averaged over the measured results are indicated at the bottom. The table includes the energy positions of the peaks reproduced with the fitting procedure and the energy levels referenced from the neutral ground state. The energy level of the $^1G_4$ state with double charge is assumed to be 218.6 eV [20–22]. Term values were calculated as the difference between this energy and the $^1G_4$·nl energy levels. It is important to note that the $^1G_4$·7d state has been identified clearly. Furthermore the corresponding states with higher quantum numbers seem to be formed slightly above the ionization threshold, which have symmetric peak shapes, different from the distorted diagram decay peaks. The state with the term value of 7.5 eV is here ascribed to the $^1G_4$·6s state, although a possibility of assigning this state to the $^1D_2$·5d or $^3F_3$·6d state cannot be ruled out (see above). From a simple approximation using the term values of the $^1G_4$·5s, $^1G_4$·5d and $^1G_4$·6d states shown in Table 1, we tried to estimate the term values for the $^1G_4$·6s, $^1D_2$·5d and $^3F_3$·6d states. The estimated values are 5.2, 7.1 and 7.8 eV, respectively. The photon energy dependence of the appearance of the state of interest, 7.5 eV term value, suggests that the loosely bound electron is an s-type orbital (see discussion on figure 5). From this consideration, it is most probable that this state is a mixed state among those states here mentioned and/or other states through correlation interaction.

In order to confirm the assignments proposed here, we have calculated effective quantum numbers (n^*) for the final states by means of the following equation:

$$T = \frac{Z^2 \times Ry}{(n^*)^2} = \frac{Z^2 \times Ry}{(n - \delta_l)^2} . \qquad (3)$$

In this equation, T denotes the term value, Z indicates the charge of the ion core and Ry is the Rydberg energy. The parameter δ_l is called the quantum defect. Table 2 lists the assignments, energy levels with respect to the ground state, term values, effective quantum numbers and quantum defects for the $^1G_4$·5s, $^1G_4$·6s and $^1G_4$·nd (n = 4–7) states. Uncertainties of the quantum defects of the $^1G_4$·6d and $^1G_4$·7d states were evaluated as 0.19 and 0.56, respectively, based on the dispersion of the term values. The values of the quantum defect proposed here are reasonable for this singly charged ion (Kr^+) in consideration of those obtained from photoabsorption spectra [17,37–39].

The yields for the resonant Auger final states are shown as a function of the photon energy in figure 5. A variety of symbols are used for the curves of individual $^1G_4$·nl final states (see figure caption). The plotting of this figure was made for average yields obtained in the parallel and perpendicular directions because of little anisotropic angular distribution measured for these final states. As expected from the total ion yield curve (figure 1), the $^1G_4$·4d state exhibits the highest intensity among the states identified. This state is found to be produced over a wide photon energy range. In particular it is of interest that this state has a considerable yield at 1685 eV, about 7 eV above the ionization threshold. Similar feature is seen for the $^1G_4$·5d state. These findings originate from the

short lifetime of the $2p_{3/2}$ hole and further are connected with the recapture of the 2p photoelectron through the PCI. The production of the $^1G_4$·5s final state, on the other hand, does not seem to continue above the ionization threshold. This finding possibly comes from the difference in the spacial distribution between the s- and d-type orbitals.

The dependence of resonant Auger yields on the direction to the photon polarization has been checked for the peak-fitting results. The angular distribution seems to be close to isotropic, although uncertainties are relatively large. This finding is related to the angular distribution of the diagram transition into the $^1G_4$ state. The observation of the $^1G_4$ decay in the present study has shown that the angular distribution is close to isotropic; the absolute value of the anisotropy parameter is lower than 0.1. A previous calculation predicts that the parameter is -0.045 [22].

4. Summary

The electron emission spectra related to the Kr $2p_{3/2}$ excitation have been measured using monochromatized undulator radiation and a hemispherical electron energy analyzer. Measured electron spectra consist of the 3p photoelectrons, normal Auger electrons and the resonant Auger peaks. The peak-fitting analysis of these spectra clarified that the electron emission into the $^1G_4$·4d final state holds the highest intensity among the resonant Auger transitions and that this transition takes place over a wide energy range of the incident photon. Other final states identified here are $^1G_4$·5s, $^1G_4$·6s and $^1G_4$·nd (n = 5, 6, 7), and the ^3F_J·4d (J = 2, 3, 4) states are found to be produced slightly.

Acknowledgments

The authors wish to express sincere thanks to the members of the research team for soft X-ray photochemistry for their fruitful comments, and to the SPring-8 facility staff for their assistance during the course of the experiments. This study was carried out with the approval of the SPring-8 Program Advisory Committee (Proposal Nos. 2001A0142-NS-np, 2002A0068-NS1-np and 2002B0507-NS1-np) and supported in part by Grants-in-Aid for Scientific Research and the Budget for Nuclear Research from the Ministry of Education, Science, Sports, Culture and Technology of Japan.

References

[1] Armen G B, Aksela H, Åberg T and Aksela S 2000 *J. Phys. B: At. Mol. Opt. Phys.* **33** R49

[2] Armen G B, Southworth S H, Levin J C, Arp U, LeBrun T and MacDonald M A 1997 *Phys. Rev. A* **56** R1079

[3] Aksela H, Kivilompolo M, Nõmmiste E and Aksela S 1997 *Phys. Rev. Lett.* **79** 4970

[4] LeBrun T, Southworth S H, Armen G B, MacDonald M A and Azuma Y 1999 *Phys. Rev. A* **60** 4667

[5] Nayandin O, Gorczyca T W, Wills A A, Langer B, Bozek J D and Berrah N 2001 *Phys. Rev. A* **64** 022505

[6] Huttula S-M, Heinäsmäki S, Aksela H, Tulkki J, Kivimäki A, Jurvansuu M and Aksela S 2001 *Phys. Rev. A* **63** 032703

[7] Camilloni R, Žitnik M, Comicioli C, Prince K C, Zacchigna M, Crotti C, Ottaviani C, Quaresima C, Perfetti P and Stefani G 1996 *Phys. Rev. Lett.* **77** 2646

[8] Rubensson J-E, Neeb M, Bringer A, Biermann M and Eberhardt W 1996 *Chem. Phys. Lett.* **257** 447

[9] Aksela H, Aksela S, Mäntykenttä A, Tulkki J, Shigemasa E, Yagishita A and Furusawa Y 1992 *Phys. Scr.* **T41** 113

[10] van der Straten P, Morgenstern R and Niehaus A 1988 *Z. Phys. D* **8** 35

[11] Russek A and Mehlhorn W 1986 *J. Phys. B: At. Mol. Phys.* **19** 911

[12] Tulkki J, Armen G B, Åberg T, Crasemann B and Chen M H 1987 *Z. Phys. D* **5** 241

[13] Mizuno J, Ishihara T and Watanabe T 1984 *J. Phys. B: At. Mol. Phys.* **17** L85

[14] Ishiguro E, Ohashi H, Lu L-j, Watari W, Kamizato M and Ishikawa T 1999 *J. Electron Spectrosc. Relat. Phenom.* **101-103** 979

[15] Tanaka T, Hara T, Oura M, Ohashi H, Kimura H, Goto S, Suzuki Y and Kitamura H 1999 *Rev. Sci. Instrum.* **70** 4153

[16] Ohashi H, Ishiguro E, Tamenori Y, Okumura H, Hiraya A, Yoshida H, Senba Y, Okada K, Saito N, Suzuki I H, Ueda K, Ibuki T, Nagaoka S, Koyano I and Ishikawa T 2001 *Nucl. Instrum. Methods A* **467-468** 533

[17] Wuilleumier F 1971 *J. Phys. (Paris)* **32** C4-88

[18] Schmelz H C, Gaveau M A, Reynaud C, Heinzel C, Baumgärtel H and Rühl E 1995 *Physica B* **208-209** 519

[19] Hayaishi T, Tanaka T, Yoshii H, Murakami E, Shigemasa E, Yagishita A, Koike F and Morioka Y 1999 *J. Phys. B: At. Mol. Opt. Phys.* **32** 1507

[20] Aksela H, Aksela S, Väyrynen J and Thomas T D 1980 *Phys. Rev. A* **22** 1116

[21] Levin J C, Sorensen S L, Crasemann B, Chen M H and Brown G S 1986 *Phys. Rev. A* **33** 968

[22] Kleiman U, Paripás B, Lohmann B, Víkor Gy and Ricz S 1999 *J. Phys. B: At. Mol. Opt. Phys.* **32** 4781

[23] Nagaoka S, Ibuki T, Saito N, Shimizu Y, Senba Y, Kamimori K, Tamenori Y, Ohashi H and Suzuki I H 2000 *J. Phys. B: At. Mol. Opt. Phys.* **33** L605

[24] Ibuki T, Okada K, Kamimori K, Sasaki J, Yoshida H, Hiraya A, Suzuki I H, Saito N, Nagaoka S, Shimizu Y, Ohashi H and Tamenori Y 2002 *Surf. Rev. Lett.* **9** 85

[25] Shimizu Y, Yoshida H, Okada K, Muramatsu Y, Saito N, Ohashi H, Tamenori Y, Fritzsche S, Kabachnik N M, Tanaka H and Ueda K 2000 *J. Phys. B: At. Mol. Opt. Phys.* **33** L685

[26] Coreno M, Avaldi L, Camilloni R, Prince K C, de Simone M, Karvonen J, Colle R and Simonucci S 1999 *Phys. Rev. A* **59** 2494

[27] Suzuki I H, Okada K, Kamimori K, Sasaki J, Yoshida H, Hiraya A, Shimizu Y, Nagaoka S, Tamenori Y, Ohashi H and Ibuki T 2002 *Surf. Rev. Lett.* **9** 63

[28] Thompson A C, Attwood D T, Gullikson E M, Howells M R, Kim K-J, Kirz J, Kortright J B, Lindau I, Pianetta P, Robinson A L, Scofield J H, Underwood J H, Vaughan D, Williams G P and Winick H 2001 *X-Ray Data Booklet, 2nd Ed.* (California: Lawrence Berkeley Natl. Lab.)

[29] Cooper J W 1993 *Phys. Rev. A* **47** 1841

[30] Kennedy D J and Manson S T 1972 *Phys. Rev. A* **5** 227

[31] Krause M O and Oliver J H 1979 *J. Phys. Chem. Ref. Data* **8** 329

[32] Jauhiainen J, Kivimäki A, Aksela S, Sairanen O-P and Aksela H 1995 *J. Phys. B: At. Mol. Opt. Phys.* **28** 4091

[33] Kuchiev M Yu and Sheinerman S A 1988 *Sov. Phys. Tech. Phys.* **32** 879

[34] Sheinerman S A, Kuhn W and Mehlhorn W 1994 *J. Phys. B: At. Mol. Opt. Phys.* **27** 5681

[35] Paripás B, Vitéz G, Víkor Gy, Tőkési K and Gulyás L 2001 *J. Phys. B: At. Mol. Opt. Phys.* **34** 3301

[36] Suzuki I H, Fujii A, Nagaoka S, Kosugi M, Okada K, Ibuki T, Samori S, Tamenori Y and Ohashi H 2004 *J. Phys. B: At. Mol. Opt. Phys.* **37** 1433

[37] Huffmann R E, Tanaka Y and Larrabee J C 1963 *Appl. Opt.* **2** 947

[38] Hayaishi T, Morioka Y, Akahori T, Watanabe M, Yagishita A and Nakamura M 1986 *Z. Phys. D* **4** 25

[39] Čubrić D, Wills A A, Comer J and MacDonald M A 1992 *J. Phys. B: At. Mol. Opt. Phys.* **25** 5069

Figures

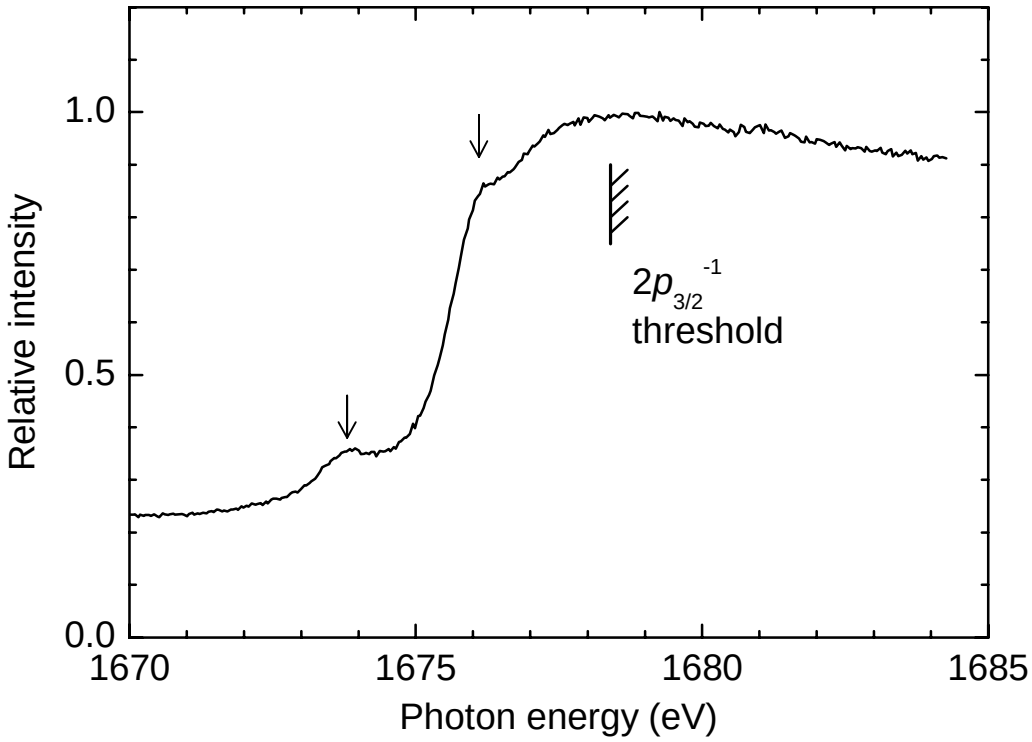

Figure 1. Total ion yield of Kr as a function of photon energy in vicinity of the $2p_{3/2}$ ionization threshold. The bar with hatching denotes the threshold. Arrows indicate the energies of the 5s and 4d orbital excitations.

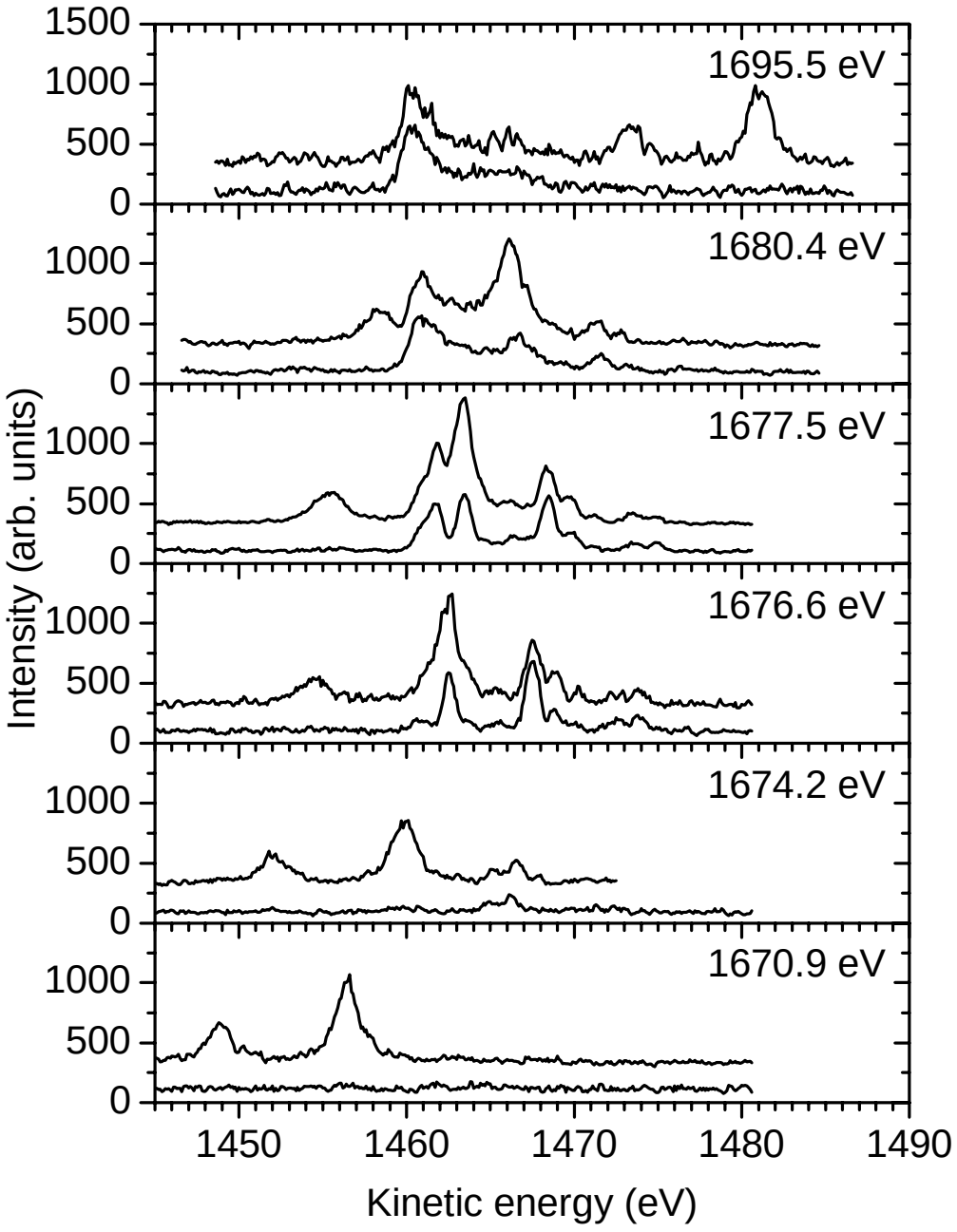

Figure 2. Electron kinetic energy spectra of Kr at several photon energies in the region of the $2p_{3/2}$ ionization threshold. The spectra in the parallel direction are drawn on a lifted baseline. The photon energy is put at the right end for each panel.

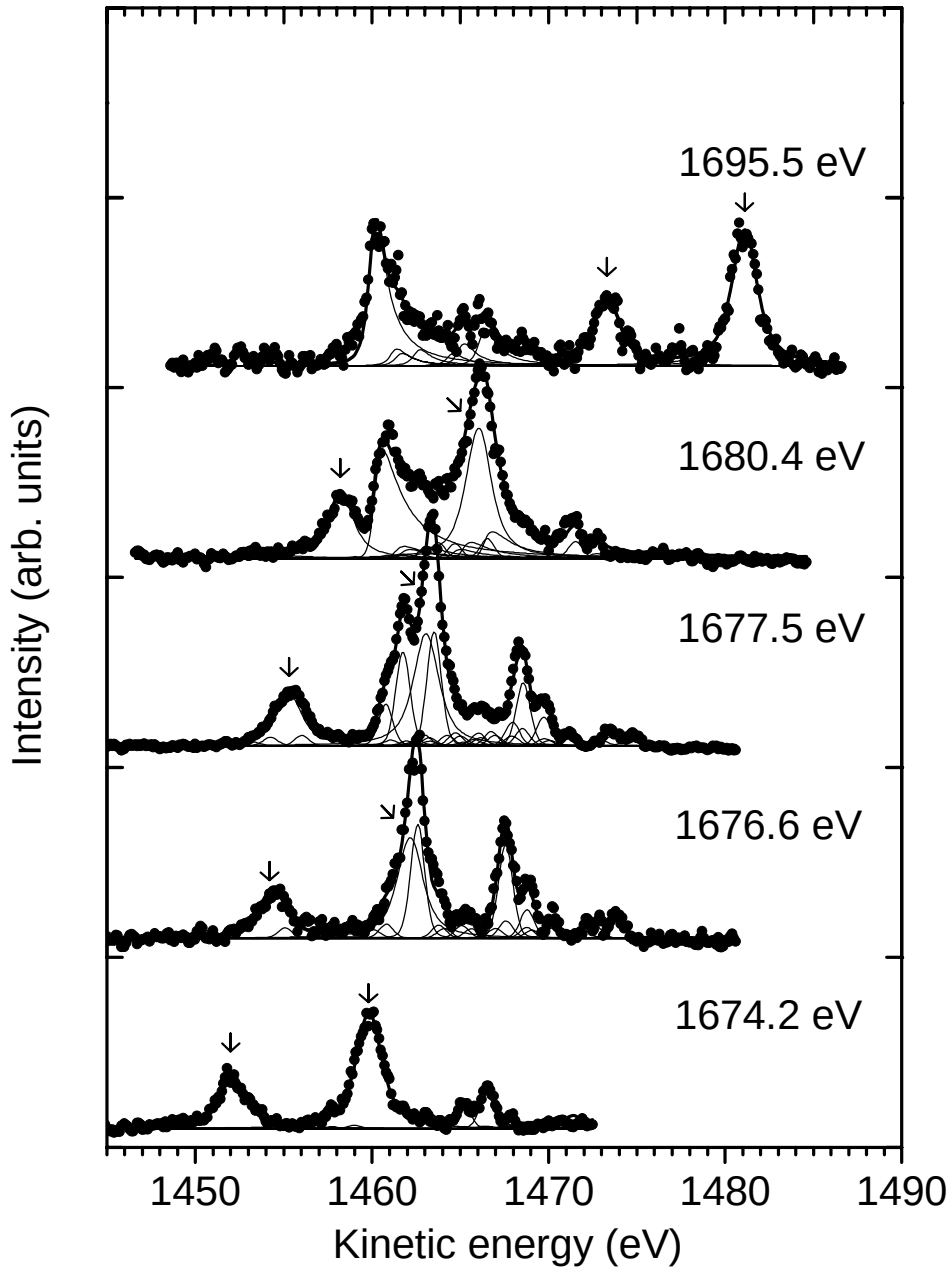

Figure 3. Reproduction of electron kinetic energy spectra for resonant Auger transitions in the parallel direction at several photon energies (1674.2, 1676.6, 1677.5, 1680.4 and 1695.5 eV). Solid circles denote measured signals, thin curves indicate profiles calculated for individual transitions and thick curves are the summation of thin curves. Arrows indicate the $3p_{1/2}$ and $3p_{3/2}$ photoelectron peaks. The photon energy is put at the right end for each panel.

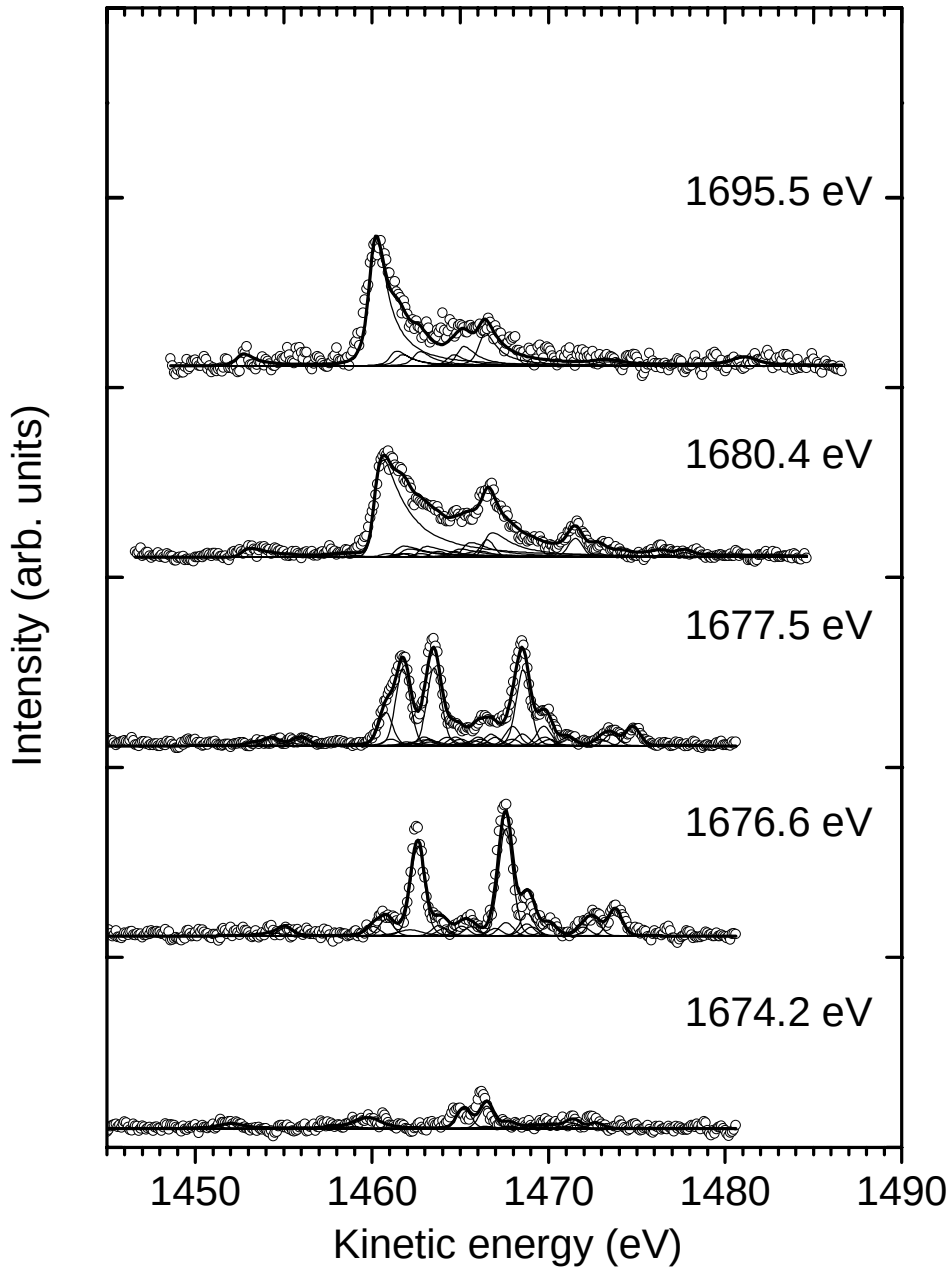

Figure 4. Reproduction of electron kinetic energy spectra for resonant Auger transitions in the perpendicular direction at several photon energies (1674.2, 1676.6, 1677.5, 1680.4 and 1695.5 eV). Solid circles denote measured signals, thin curves indicate profiles calculated for individual transitions and thick curves are the summation of thin curves. The photon energy is put at the right end for each panel.

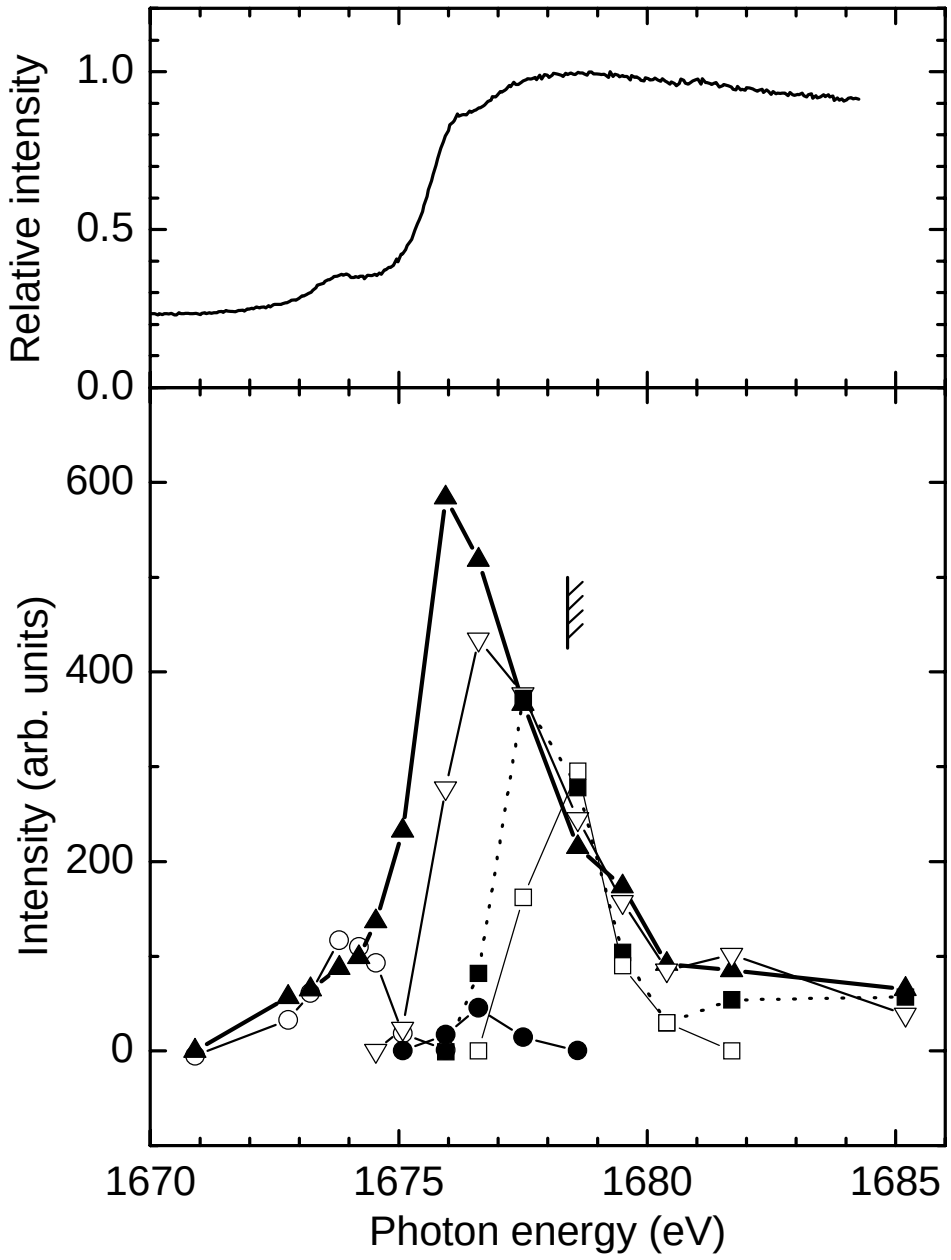

Figure 5. Photon energy dependence of resonant Auger transitions into $^1G_4$·nl final states in vicinity of the $2p_{3/2}$ ionization threshold. The bar with hatching denotes the threshold. Uncertainties for the plotted data are about 10% for those with high intensities, and those are 30% or more for low intensity ones. Symbols are: ○, $^1G_4$·5s; ●, $^1G_4$·6s; ▲, $^1G_4$·4d; ▽, $^1G_4$·5d; ■, $^1G_4$·6d; and □, $^1G_4$·7d. Total ion yield of Kr is also shown in the upper panel.

Table 1. Electron kinetic energies (upper rows), energy levels (lower rows) and term values (bottom) of resonant Auger final states expressed with $^1G_4$·nl (in units of eV).

Photon energy (eV)	5s	4d	6s	5d	6d	7d	Higher orbitals
1674.2	1466.5	1465.2	–	–	–	–	–
	207.7	209.0	–	–	–	–	–
1676.0	1468.4	1467.2	1464.8	1462.2	1460.5	–	–
	207.6	208.8	211.2	213.8	215.5	–	–
1676.6	–	1467.6	1465.6	1462.6	1460.8	–	–
	–	209.0	211.0	214.0	215.8	–	–
1677.5	–	1468.6	1466.5	1463.5	1461.8	1460.8	–
	–	208.9	211.0	214.0	215.7	216.7	–
1678.6	–	1469.5	–	1464.5	1462.8	1461.3	–
	–	209.1	–	214.1	215.8	217.3	–
1679.5	–	1470.4	–	1465.4	1463.5	1462.5	1461.3
	–	209.1	–	214.1	216.0	217.0	218.2
	11.0	9.6	7.5	4.6	2.8	1.6	0.4

Table 2. Energy levels, term values and quantum defects for the $^1G_4$·nl states of Kr^+ (in units of eV).

Assignment	Energy level	Term value	Effective quantum number	Quantum defect
$^1G_4$·5s	207.6	11.0	2.23	2.77
$^1G_4$·4d	209.0	9.6	2.38	1.62
$^1G_4$·6s	211.1	7.5	2.69	3.31
$^1G_4$·5d	214.0	4.6	3.44	1.56
$^1G_4$·6d	215.8	2.8	4.38	1.62
$^1G_4$·7d	217.0	1.6	5.83	1.17